Diagnosis of dynamic process over rainband of landfall typhoon*

Ran Ling-Kun(冉令坤)[a)†], Yang Wen-Xia(杨文霞)[b)c)], and Chu Yan-Li(楚艳丽)[d)]

[a)] *Institute of Atmospheric Physics, Chinese Academy of Sciences, Beijing* 100029, *China*
[b)] *Hebei Weather Modification Office, Shijiazhuang* 050021, *China*
[c)] *Hebei Laboratory of Ecological and Enviromental Monitoring, Shijiazhuang* 050021, *China*
[d)] *Institute of Urban Meteorology, CMA, Beijing* 100089, *China*

(Received 4 July 2009; revised manuscript received 15 November 2009)

This paper introduces a new physical parameter — thermodynamic shear advection parameter combining the perturbation vertical component of convective vorticity vector with the coupling of horizontal divergence perturbation and vertical gradient of general potential temperature perturbation. For a heavy-rainfall event resulting from the landfall typhoon 'Wipha', the parameter is calculated by using National Centres for Enviromental Prediction/National Centre for Atmospheric Research global final analysis data. The results showed that the parameter corresponds to the observed 6 h accumulative rainband since it is capable of catching hold of the dynamic and thermodynamic disturbance in the lower troposphere over the observed rainband. Before the typhoon landed, the advection of the parameter by basic-state flow and the coupling of general potential temperature perturbation with curl of Coriolis force perturbation are the primary dynamic processes which are responsible for the local change of the parameter. After the typhoon landed, the disturbance is mainly driven by the combination of five primary dynamic processes. The advection of the parameter by basic-state flow was weakened after the typhoon landed.

Keywords: thermodynamic shear advection parameter, convective vorticity vector, horizontal divergence, general potential temperature

PACC: 9260, 9260D, 9260V, 9260X

1. Introduction

It has been a long time since meteorologists paid much attention to the forecast of locations and moving directions of precipitable weather systems.[1,2] Many important macroscopical physical parameters were proposed to diagnose formation mechanism of heavy-rainfall events.[3,4] The typical parameters, such as helicity describing synthetically fluid rotation and intensity along rotary direction and potential vorticity representing comprehensively fluid rotation and thermodynamic transport effect, are successfully applied to interpret atmospheric phenomena and a great achievement has been reached. Wu *et al.*[5] demonstrated that helicity is conservative for an isentropic fluid. It was manifested in many studies that helicity is a valid tracer to detect disastrous weather such as thunderstorm, tornado, large-scale rainstorm and sand storm.[6−9] Unlike convective available potential energy (CAPE) and Richardson number denoting potential instable energy and potential instability, respectively, helicity coupling velocity and vorticity, well describe dynamic breakout of potential instability. So helicity is more directly connected with heavy precipitation.

Since the concept of potential vorticity is first introduced by Ertel,[10] it has been widely applied to investigating large-scale cyclone in the mid-high latitudes. Many outstanding works associated with potential vorticity have been done and great achievements are obtained in understanding the physical processes of atmospheric circulations.[11−14] However, potential vorticity encounters a limitation and is a weak signal when it is applied to the equatorial deep convections in two-dimensional atmosphere. The reason is that the potential vorticity in two-dimensional atmosphere is expressed as $\omega_{\rm a} \cdot \nabla\theta/\rho = (2\Omega \sin\varphi/\rho)(\partial\theta/\partial z)$, and it is equal to zero at equator due to $\varphi = 0$.[15] After being cognizant of the limitation of potential vorticity, Gao *et al.*[15,16] introduced the concept of two-dimensional convective vorticity

*Project supported by the National Basic Research Program of China (Grant No. 2009CB421505), the Main Direction Program of Knowledge Innovation of Chinese Academy of Sciences (KZCX2-YW-206-4), the National Natural Science Foundation of China (Grant Nos. 40875032 and 40875002), the Major Foreland Project of IAP (IAP07201) and the National Science and Technology Project, China (GYH200706042).

†Corresponding author. E-mail: rlk@mail.iap.ac.cn

© 2010 Chinese Physical Society and IOP Publishing Ltd

vector (CVV) and employed it to diagnose the equatorial deep convections. Their results showed that the vertical component of CVV was correlated highly with the cloud hydrometeors simulated by cloud-resolving model. This implies that CVV may effectively represent the evolution of equatorial deep convection systems. After that, Gao *et al.*[17] and Cui[18] further generalised CVV to a three-dimensional situation and investigated the relation between CVV and convections in the three-dimensional environment. Since the concept of CVV was proposed by Gao *et al.*,[15] it has been more and more used in the diagnosis of convection and typhoon. On the other hand, CVV is a vector and its three components are different in order of magnitude and physical meaning. So it is not an easy task to choose which component of CVV to diagnose in practice.

Since the above three typical macroscopical physical parameters are composed by total variables which are not divided into a basic-state portion and a perturbation portion, they may depict the complete dynamic and thermodynamic characteristics of circulations. Generally, precipitable weather system is regarded as a disturbance imposed on background environment. So a parameter completely composed by perturbation fields may be more suitable for describing precititable weather systems.

The purpose of this paper is to introduce a thermodynamic shear advection parameter (TSAP) on the basis of CVV and use it to diagnose the dynamic process over rainband of landfall typhoon. The TSAP is only constituted by perturbation fields and quadric in disturbance amplitude. So TSAP in nature is a wave-activity density which generally is defined as a disturbance quantity quadric or higher-order in disturbance amplitude in the small-amplitude limit and is widely used to study wave propagation[20,21] and wave-mean flow interaction.[22,23] The definition of TSAP and its tendency equation are addressed in Section 2. In Section 3, TSAP is calculated to analyse the dynamic process responsible for the observed rainband of landfall typhoon 'Wipha' with the National Centres for Enviromental Prediction/National Centre for Atmospheric Research (NCEP/NCAR) global final analysis data. Besides this, the chief dynamic factors influencing the development of TSAP is also investigated. The conclusion is given in Section 4.

2. Thermodynamic shear advection parameter

For a three-dimensional, inviscid, diabatic, rotational and hydrostatic flow, the governing equations on f plane in pressure coordinates (x, y, p, t) are given by

$$\frac{\mathrm{d}u}{\mathrm{d}t} - fv = -\frac{\partial \phi}{\partial x}, \tag{1}$$

$$\frac{\mathrm{d}v}{\mathrm{d}t} + fu = -\frac{\partial \phi}{\partial y}, \tag{2}$$

$$\frac{\partial \phi}{\partial p} = -\frac{1}{\rho}, \tag{3}$$

$$\nabla \cdot \boldsymbol{v} = 0, \tag{4}$$

$$\frac{\mathrm{d}\theta}{\mathrm{d}t} = S_\theta, \tag{5}$$

$$\frac{\mathrm{d}q_v}{\mathrm{d}t} = S_{q_v}, \tag{6}$$

$$p = \rho RT\left(1 + \lambda q_v\right), \tag{7}$$

$$\theta = T\left(\frac{p_s}{p}\right)^{R/c_p}, \tag{8}$$

where $\boldsymbol{v} = (u,\ v,\ \omega)$ is the three-dimensional velocity vector, ϕ is the geopotential height, f is the constant Coriolis parameter, θ is the potential temperature, S_θ is the diabiatic heating rate, p is the pressure, ρ is the density, p_s is the reference pressure, T is the temperature, R is the dry gas constant, c_p is the specific heat at constant pressure, q_v is the specific humidity, S_{q_v} is the source or sink of q_v, $\lambda = 0.61$ a constant, $\mathrm{d}/\mathrm{d}t = \partial/\partial t + \boldsymbol{v} \cdot \nabla$ and $\nabla = (\partial/\partial x)\boldsymbol{i} + (\partial/\partial y)\boldsymbol{j} + (\partial/\partial p)\boldsymbol{k}$.

Gao *et al.* firstly proposed the concept of general potential temperature[19]

$$\theta^* = \theta \exp\left[\frac{L_v q_{vs}}{c_p T_\mathrm{c}}\left(\frac{q_v}{q_{vs}}\right)^k\right], \tag{9}$$

where q_{vs} is the saturated specific humidity, T_c is the temperature at condensation lift level, and k is an experiential constant. Since then, the general potential temperature has been more and more used in diagnosis of convection cloud and heavy-rainfall event. Many studies manifested that the general potential temperature is capable of representing more exactly the thermodynamic status of real atmosphere. Based on the thermodynamic equation (5), the equation for general potential temperature may be derived,

$$\frac{\mathrm{d}\theta^*}{\mathrm{d}t} = S_{\theta^*}, \tag{10}$$

where

$$S_{\theta^*} = \frac{\theta^*}{\theta} S_\theta + \theta^* \ln\left(\frac{\theta^*}{\theta}\right)\left[k\frac{\mathrm{d}}{\mathrm{d}t}(\ln q_v) + (1-k)\frac{\mathrm{d}}{\mathrm{d}t}(\ln q_{vs}) - \frac{\mathrm{d}}{\mathrm{d}t}(\ln T_c)\right]$$

is the source or sink of θ^*.

Assuming that a variable may be decomposed into a basic-state portion (denoted by the subscript '0') and a perturbation portion (denoted by the subscript 'e'), one has

$$u = u_0 + u_e, \quad v = v_0 + v_e, \quad w = w_0 + w_e,$$
$$\phi = \phi_0 + \phi_e, \quad \theta^* = \theta_0^* + \theta_e^*. \tag{11}$$

Accordingly, the basic-state equations and linear perturbation equations are given by

$$\frac{\partial u_0}{\partial t} + \boldsymbol{v}_0 \cdot \nabla u_0 - f v_0 = -\frac{\partial \phi_0}{\partial x}, \tag{12}$$
$$\frac{\partial v_0}{\partial t} + \boldsymbol{v}_0 \cdot \nabla v_0 + f u_0 = -\frac{\partial \phi_0}{\partial y}, \tag{13}$$
$$\nabla \cdot \boldsymbol{v}_0 = 0, \tag{14}$$
$$\frac{\partial \theta_0^*}{\partial t} + \boldsymbol{v}_0 \cdot \nabla \theta_0^* = 0, \tag{15}$$
$$\frac{\partial u_e}{\partial t} = -\boldsymbol{v}_e \cdot \nabla u_0 - \boldsymbol{v}_0 \cdot \nabla u_e + f v_e - \frac{\partial \phi_e}{\partial x}, \tag{16}$$
$$\frac{\partial v_e}{\partial t} = -\boldsymbol{v}_e \cdot \nabla v_0 - \boldsymbol{v}_0 \cdot \nabla v_e - f u_e - \frac{\partial \phi_e}{\partial y}, \tag{17}$$
$$\nabla \cdot \boldsymbol{v}_e = 0, \tag{18}$$
$$\frac{\partial \theta_e^*}{\partial t} = -\boldsymbol{v}_e \cdot \nabla \theta_0^* - \boldsymbol{v}_0 \cdot \nabla \theta_e^* + S_{\theta^*}, \tag{19}$$

where $\boldsymbol{v}_e = (u_e,\ v_e,\ \omega_e)$ is the three-dimensional velocity vector perturbation and $\boldsymbol{v}_0 = (u_0,\ v_0,\ \omega_0)$ is the three-dimensional basic-state velocity vector.

In the pressure coordinates, a perturbation scalar quadric in disturbance fields is introduced

$$M = -\frac{\partial \boldsymbol{v}_e}{\partial p} \cdot \nabla \theta_e^*. \tag{20}$$

By using Eq. (18), one may transform the perturbation scalar Eq. (20) into

$$M = -\left(\frac{\partial u_e}{\partial p}\frac{\partial \theta_e^*}{\partial x} + \frac{\partial v_e}{\partial p}\frac{\partial \theta_e^*}{\partial y}\right) + \left(\frac{\partial u_e}{\partial x} + \frac{\partial v_e}{\partial y}\right)\frac{\partial \theta_e^*}{\partial p}. \tag{21}$$

Since Eq. (21) includes the general potential temperature perturbation, it represented the synthetical covariance of dynamic processes and thermodynamic processes. The first term on the right-hand side of Eq. (21) is analogous to the perturbation vertical component of CVV (for short PVC). The second term presents the coupling of horizontal divergence perturbation with vertical gradient of general potential temperature perturbation (for short CHV). Since the lower-level horizontal convergence and upper-level divergence are remarkable dynamic properties of atmosphere in heavy-rainfall event, the coupling term may play an important role in evolution of precipitable weather systems. Thus, the scalar may be regarded as a supplement to PVC.

The perturbation scalar M can be further rewritten as

$$M = [\nabla \times (\boldsymbol{k} \times \boldsymbol{v}_{he})] \cdot \nabla \theta_e^*, \tag{22}$$

where $\boldsymbol{v}_{he} = (u_e,\ v_e,\ 0)$ is the horizontal velocity vector perturbation. The expression of Eq. (22) is analogous to the perturbation potential vorticity in pressure coordinates

$$q_e = (\nabla \times \boldsymbol{v}_{he}) \cdot \nabla \theta_e^*. \tag{23}$$

The difference between Eqs. (22) and (23) is that the perturbation scalar M involves the perturbation vector $(\boldsymbol{k} \times \boldsymbol{v}_{he})$ instead of $\boldsymbol{v}_{he}$. The analogy of Eqs. (22) and (23) suggests that M and q_e share the same property that they have no contributions to the monochromatic wave in a uniform basic flow, unless the wave train whose amplitude, wave number, and frequency slowly vary is imposed on a non-uniform basic flow. The reason is that when the plane wave solution, $(u_e, v_e, \theta_e^*) = (U, V, \Theta)\exp[\mathrm{i}(kx + ly + np - \omega t)]$, is substituted into Eqs. (22) and (23), M and q_e are equal to zero in the limit of small amplitude.

Since the perturbation scalar M is quadric-order in disturbance fields, it can be used to diagnose the evolution of disturbance imposed on a basic flow. However, the fact that the sign of M is indefinite may mitigate the usefulness of M in practice. Therefore, it is more appropriate to consider the absolute value of M than itself, namely

$$|M| = \sqrt{M^2}. \tag{24}$$

Because $|M|$ is always definitely positive in sign, $|M|$ is capable of describing a kind of perturbation energy and represents the disturbance strength. So the absolute value of M is interpreted as TSAP.

On the other hand, Eq. (21) may be expressed in a flux form as follows:

$$M = -\left[\frac{\partial}{\partial x}\left(\theta_e^*\frac{\partial u_e}{\partial p}\right) + \frac{\partial}{\partial y}\left(\theta_e^*\frac{\partial v_e}{\partial p}\right)\right] + \frac{\partial}{\partial p}\left[\theta_e^*\left(\frac{\partial u_e}{\partial x} + \frac{\partial v_e}{\partial y}\right)\right]. \tag{25}$$

Taking a partial derivative with respect to time for the both sides of Eq. (25), one has

$$\begin{aligned}\frac{\partial |M|}{\partial t} = & -\frac{\partial}{\partial x}\left[\frac{M}{|M|}\left(\frac{\partial \theta_{\rm e}^*}{\partial t}\frac{\partial u_{\rm e}}{\partial p}+\theta_{\rm e}^*\frac{\partial^2 u_{\rm e}}{\partial p \partial t}\right)\right] \\ & -\frac{\partial}{\partial y}\left[\frac{M}{|M|}\left(\frac{\partial \theta_{\rm e}^*}{\partial t}\frac{\partial v_{\rm e}}{\partial p}+\theta_{\rm e}^*\frac{\partial^2 v_{\rm e}}{\partial p \partial t}\right)\right] \\ & +\frac{\partial}{\partial p}\left\{\frac{M}{|M|}\left[\frac{\partial \theta_{\rm e}^*}{\partial t}\left(\frac{\partial u_{\rm e}}{\partial x}+\frac{\partial v_{\rm e}}{\partial y}\right)\right.\right. \\ & \left.\left.+\theta_{\rm e}^*\left(\frac{\partial^2 u_{\rm e}}{\partial x \partial t}+\frac{\partial^2 v_{\rm e}}{\partial y \partial t}\right)\right]\right\}. \qquad (26)\end{aligned}$$

In the derivation of Eq. (26), we use the following relations

$$\frac{\partial |M|}{\partial t} = \frac{M}{|M|}\frac{\partial M}{\partial t}, \qquad (27)$$

$$\frac{\partial}{\partial x}\left(\frac{M}{|M|}\right) = 0, \qquad (28)$$

$$\frac{\partial}{\partial y}\left(\frac{M}{|M|}\right) = 0, \qquad (29)$$

$$\frac{\partial}{\partial p}\left(\frac{M}{|M|}\right) = 0. \qquad (30)$$

After eliminating the local changes of perturbation fields in Eq. (26) with the linear perturbation equations (16)–(19), one may obtain the tendency equation of $|M|$ in pressure coordinates

$$\frac{\partial |M|}{\partial t} = \nabla \cdot \boldsymbol{F} + \nabla\left(\frac{M}{|M|}S_{\theta_{\rm e}^*}\frac{\partial}{\partial p}\boldsymbol{v}_{\rm e}\right), \qquad (31)$$

where

$$\boldsymbol{F} = \boldsymbol{F}_1 + \boldsymbol{F}_2 + \boldsymbol{F}_3 + \boldsymbol{F}_4 + \boldsymbol{F}_5 \qquad (32)$$

is the flux vector quadric in disturbance fields. The five portions in Eq. (32) are given by

$$\boldsymbol{F}_1 = -\boldsymbol{v}_0 |M|, \qquad (33)$$

$$\begin{aligned}\boldsymbol{F}_2 = & \frac{M}{|M|}\theta_{\rm e}^*[\nabla u_0 \times \nabla v_{\rm e} + \nabla u_{\rm e} \times \nabla v_0 \\ & + \nabla \times (\boldsymbol{v}_{\rm adv} \times \boldsymbol{k})], \qquad (34)\end{aligned}$$

$$\boldsymbol{F}_3 = \frac{M}{|M|}(\boldsymbol{v}_{\rm e} \cdot \nabla \theta_0^*)\frac{\partial}{\partial p}\boldsymbol{v}_{\rm e}, \qquad (35)$$

$$\boldsymbol{F}_4 = \frac{M}{|M|}\theta_{\rm e}^* \nabla \times (f \boldsymbol{v}_{\rm he}), \qquad (36)$$

$$\boldsymbol{F}_5 = \frac{M}{|M|}\theta_{\rm e}^* \nabla \times (\nabla \varphi_{\rm e} \times \boldsymbol{k}), \qquad (37)$$

where $\boldsymbol{v}_{\rm adv} = \boldsymbol{v}_{\rm e} \cdot \nabla u_0 \boldsymbol{i} + \boldsymbol{v}_{\rm e} \cdot \nabla v_0 j + \boldsymbol{v}_{\rm e} \cdot \nabla w_0 \boldsymbol{k}$ is the linear perturbation vector composed of basic-state velocity advection by velocity vector perturbation. The second term on the right-hand side of Eq. (31) is referred to as the source or sink of $|M|$ that comes from the coupling of source or sink of general potential temperature with vertical shears of velocity vector perturbation. Since both $|M|$ and $\boldsymbol{F}$ are quadric in disturbance fields and Eq. (31) takes a local flux form, Eq. (31) in nature is a wave-activity law. The $|M|$ and $\boldsymbol{F}$ are equivalent to the wave-activity density and wave-activity flux divergence, respectively. Furthermore, the wave-activity density is not conserved due to the source or sink of general potential temperature.

The three-dimensional flux $\boldsymbol{F}$ in Eq. (31) is composed of five portions. $\boldsymbol{F}_1$ denotes the advection transport of $|M|$ by basic-state velocity vector. The $\boldsymbol{F}_2$ is the term coupling of general potential temperature perturbation with covariance between basic-state flow and velocity perturbation. The $\boldsymbol{F}_3$ is related to the interaction between the basic-state general potential temperature advection by velocity vector perturbation and vertical shear of velocity perturbation. The $\boldsymbol{F}_4$ represents the coupling of general potential temperature perturbation with curl of Coriolis force perturbation. The $\boldsymbol{F}_5$ indicates the influence of interaction between general potential temperature perturbation and horizontal gradients of geopotential height perturbation on the local change of $|M|$.

Since $|M|$, quadric in disturbance fields, completely composes of perturbation variables and excludes any basic-state variable, it may represent the strength of a disturbance. Since $\boldsymbol{F}$, quadric in disturbance fields, involves basic-state fields as well as linear perturbation variables, it may denote the interaction between wave and basic-state flow. Therefore, the Eq. (31) describes contribution of wave-basic flow interaction to evolution of disturbance. Since the perturbation scalar $|M|$ can catch hold of the dynamic and thermodynamic properties of precipitable weather systems, theoretically the perturbation scalar may be used to analyse disturbance leading to heavy rainfall. In order to verify the validity of $|M|$ in practice, it will be employed to diagnose dynamic process responsible for rainband of landfall typhoon with the NCEP/NCAR global final analysis data in the following section. Since $|M|$ is expressed entirely in terms of Eulerian quantities so that it is easily calculated with the atmospheric grid data.

3. Analysis

A heavy-rainfall event resulting from the landfall typhoon 'Wipha' occurred in the east of China during 12 universal time coordinated (UTC) 18–12 UTC 20 September 2007. The typhoon 'Wipha' originated

a disturbed weather area forming the southeast of Naha, Okinawa early on 13 September 2007. A tropical cyclone formation alert (TCFA) was issued late on September 14. The storm was upgraded to a tropical depression on September 15. On September 16, the storm had gained enough organisation to be designated as a tropical storm. On September 17, the storm underwent rapid intensification and quickly strengthened into a typhoon named 'Wipha'. It continued to strengthen rapidly and was upgraded by the JTWC to a super typhoon early on September 18. At 18 UTC 18, 'Wipha' slammed into Cangnan Country, Zhejiang Province in China with the maximum surface velocity 45 m/s. After 'Wipha' made landfall, it was weakened slightly, and became a Category 3-equivalent typhoon. The 'Wipha' continued to move northeastwards and came into Huang Sea at 23 UTC 19 after passing Anhui, Jiangsu and Shandong provinces.

For the heavy-rainfall event, $|M|$ and $\nabla \cdot \boldsymbol{F}$ in Eq. (31) were calculated by using the NCEP/NCAR global final analysis data ($1^\circ \times 1^\circ$ horizontal resolution, 26 vertical pressure levels, 6-hour time intervals). In virtue of the calculation, the dynamic process associated with the rainband in 'Wipha' was analysed. Since the global final analysis data on grid was coarse in temporal resolution and contained little information about diabatic heating and phase change of water substances, the local change of $|M|$ and source or sink in Eq. (31) were excluded from evaluation. The key problem in the calculation is how to get the basic-state fields and perturbation fields from the final analysis data. The Cressman interpolating technique was used to continuously smooth the final analysis data for 3 times with a horizontal scanning radius of about 285 km. The smoothed fields were interpreted as the basic-state fields. The perturbation fields were obtained by subtracting the basic-state fields from the final analysis data.

In order to investigate the property of TSAP on the whole, the vertical integration (denoted by $\langle \bullet \rangle = -\int_{p_s}^{p_t} \bullet \mathrm{d}p$, where $p_s = 1000$ hPa, and $p_t = 100$ hPa) was taken for $|M|$ and was presented in Figs. 1 and 2. As it was shown in Fig. 1(a), the typhoon 'Wipha' was approaching the east coast of Zhejiang Province at 12 UTC 18 Sep. 2007 and its centre was staying on the Eastern Sea near (26°N, 122°E). The central pressure of 'Wipha' was lower than 991 hPa and was accompanied with cyclonic basic-state and perturbed circulations on 850 hPa. As it was shown in Fig. 2(a), the observed 6 h accumulative rainband presented a scattered spiral shape and bended to right from the east coast of Zhejiang Province to the southwest of Jilin Province. Meantime, the anomalous region of $\langle |M| \rangle$ took a curly-band shape and overlapped the observed rainband. The positive-value band of $\langle |M| \rangle$ with a centre located near (33°N, 122°E) stretched curlily from the typhoon centre to the southwest of Jilin Province (42°N, 125°E). Another important character was that both the bands of observed rainfall and $\langle |M| \rangle$ occurred in the convergent regions of basic-state and perturbed horizontal winds on 850 hPa. The observed rainband fell into the band of $\langle |M| \rangle$. Furthermore, the rainfall centre near (33°N, 122°E) was accorded with the centre of $\langle |M| \rangle$. This indicated that there was a remarkable dynamic and thermodynamic disturbance over the observed rainband resulting from 'Wipha'. At 18 UTC 18 (Figs. 1(b) and 2(b)), the typhoon began to land the east coast of Zhejiang Province near (27°N, 120°E) and the curly band of $\langle |M| \rangle$covering the observed rainband moved northeastwards. During the period of 18 UTC 18–06 UTC 19 (Figs. 1(d) and 2(d)) when 'Wipha' landed, the band of $\langle |M| \rangle$ increased its curvature near (33°N, 120°E). At the same time, the heavy-rainfall region in the east of China moved northwards and the northeastern heavy-rainfall region transferred southwards. Thus, the bended rainband matched with the curly band of $\langle |M| \rangle$. In the course of 'Wipha' landing, the rainfall was fluctuated and the pressure of typhoon centre gradually increased, but the magnitude of $\langle |M| \rangle$ did not violently change, and its peak varied in the range of 2×10^{-3} K$\cdot$ s^{-1} and 3×10^{-3} K$\cdot$ s^{-1}. At 12 UTC 19 (Figs. 1(e) and 2(e)), the typhoon centre arrived near (32°N, 119°E) with the central pressure lower 1002 hPa. The band of $\langle |M| \rangle$ presented a hook shape stretching from the southeast of the typhoon centre to the Korea peninsula. The heavy-rainfall centre near the peak of $\langle |M| \rangle$ was located in the southern edge of the typhoon centre. At the same time, the strong precipitation region in the east of China propagated northwards with increasing rainfall, while the rainfall region in the northeast of China vanished. The high-value band of $\langle |M| \rangle$ overlapped the heavy-rainfall region with 3×10^{-3} K$\cdot$s^{-1} contour. After that, the hook-shape band of $\langle |M| \rangle$ was gradually evolved to a straight band with a southwest-northeast orientation at 06 UTC 20. Following the channel of $\langle |M| \rangle$, the landfall typhoon with gradually increasing central pressure moved northeastwards along a hook-shape routine. In the same period, the heavy-rainfall region was always collocated well with the high value of $\langle |M| \rangle$.

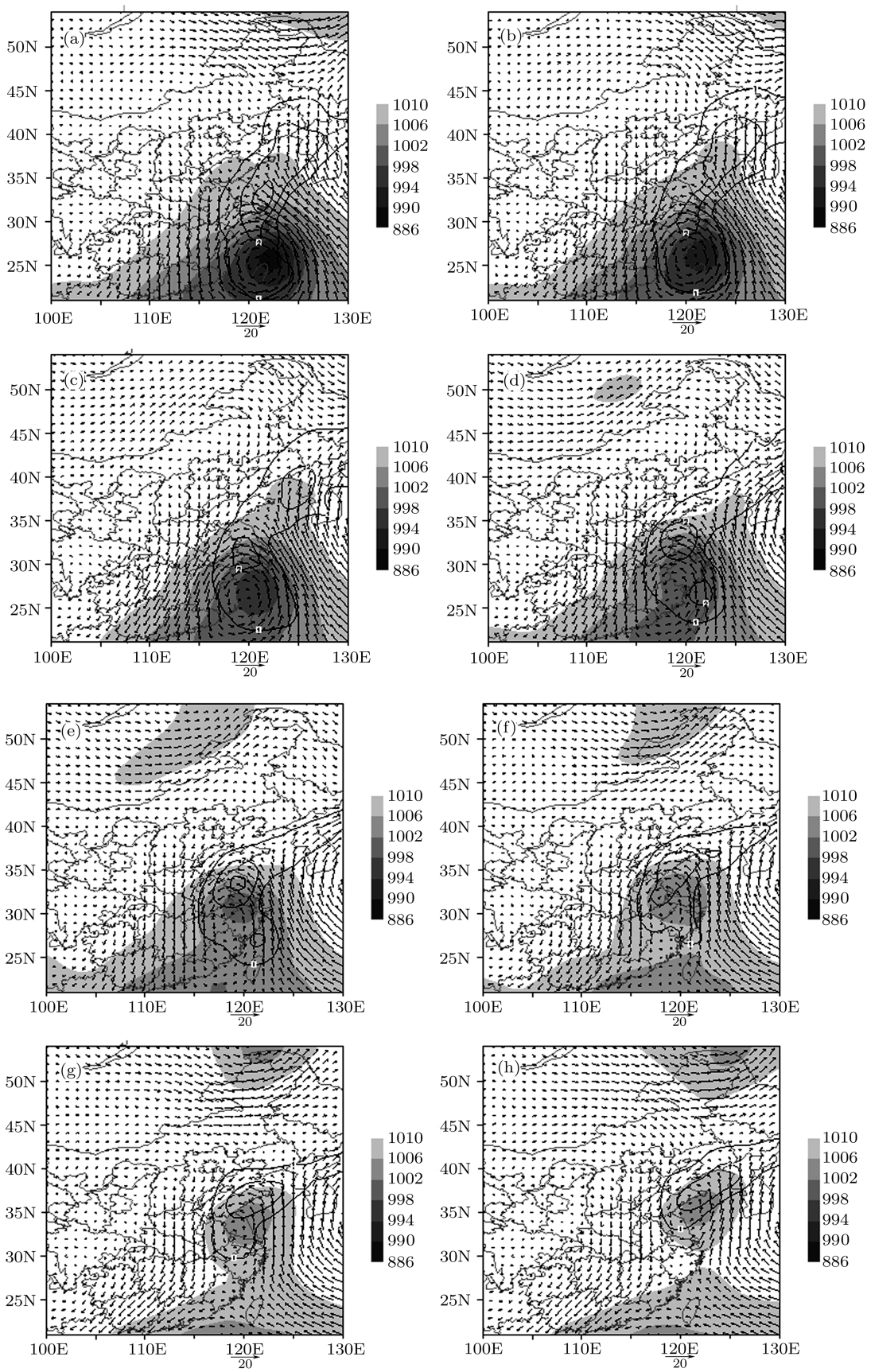


Fig. 1. The horizontal distributions of $\langle|M|\rangle$ (solid contour, unit: 10^{-3} K$\cdot$s^{-1}, sea-level pressure (grey shade, unit: hPa) and basic-state horizontal velocity vector on 850 hPa level (unit: m$\cdot$s^{-1}) at 12 UTC (a), 18 UTC 18 (b), 00 UTC (c), 06 UTC (d), 12 UTC (e), 18 UTC 19 (f), 00 UTC (g) and 06 UTC 20 (h) Sep. 2007. The ordinate is the latitude and the abscissa is the longitude.

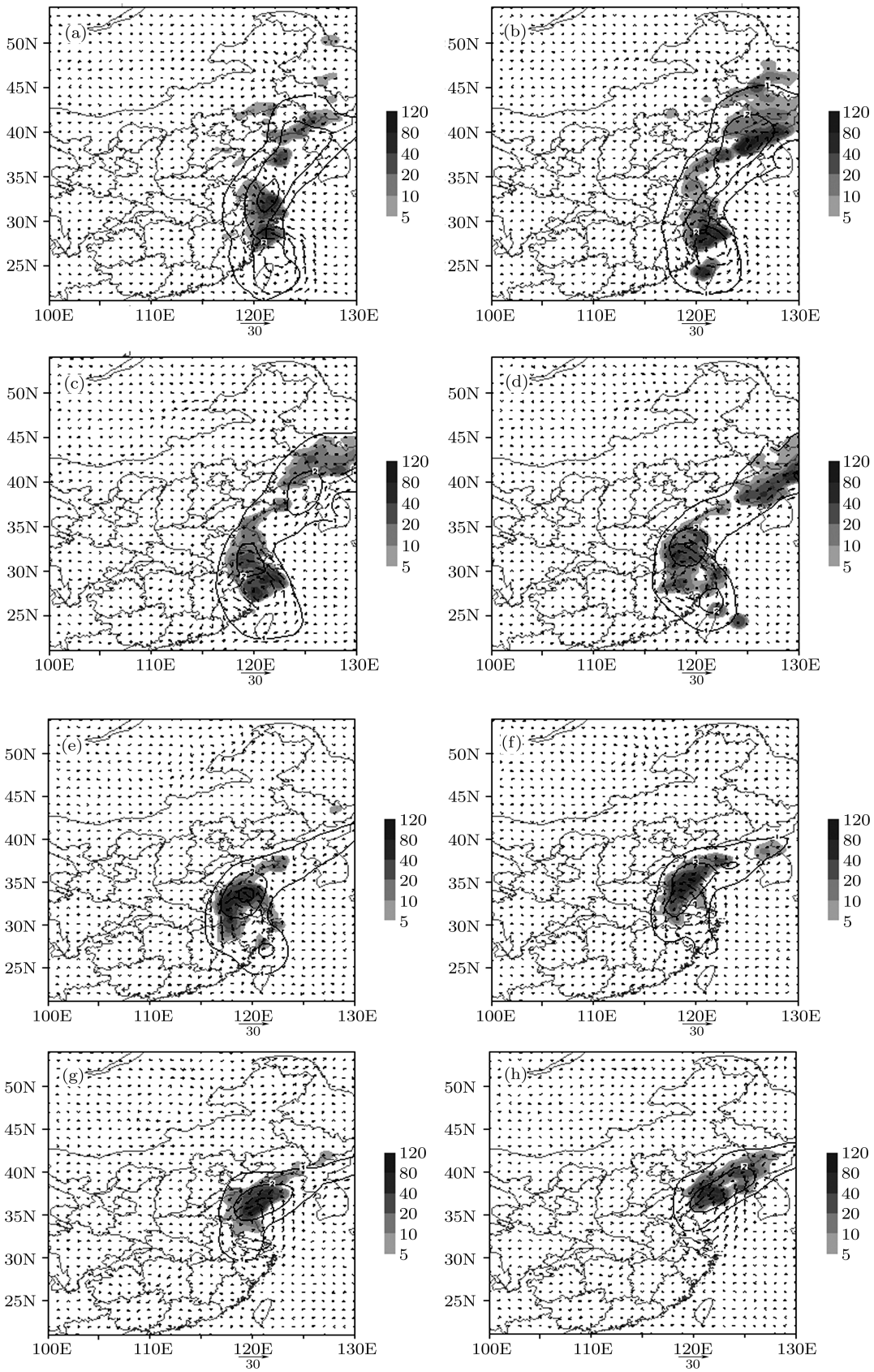
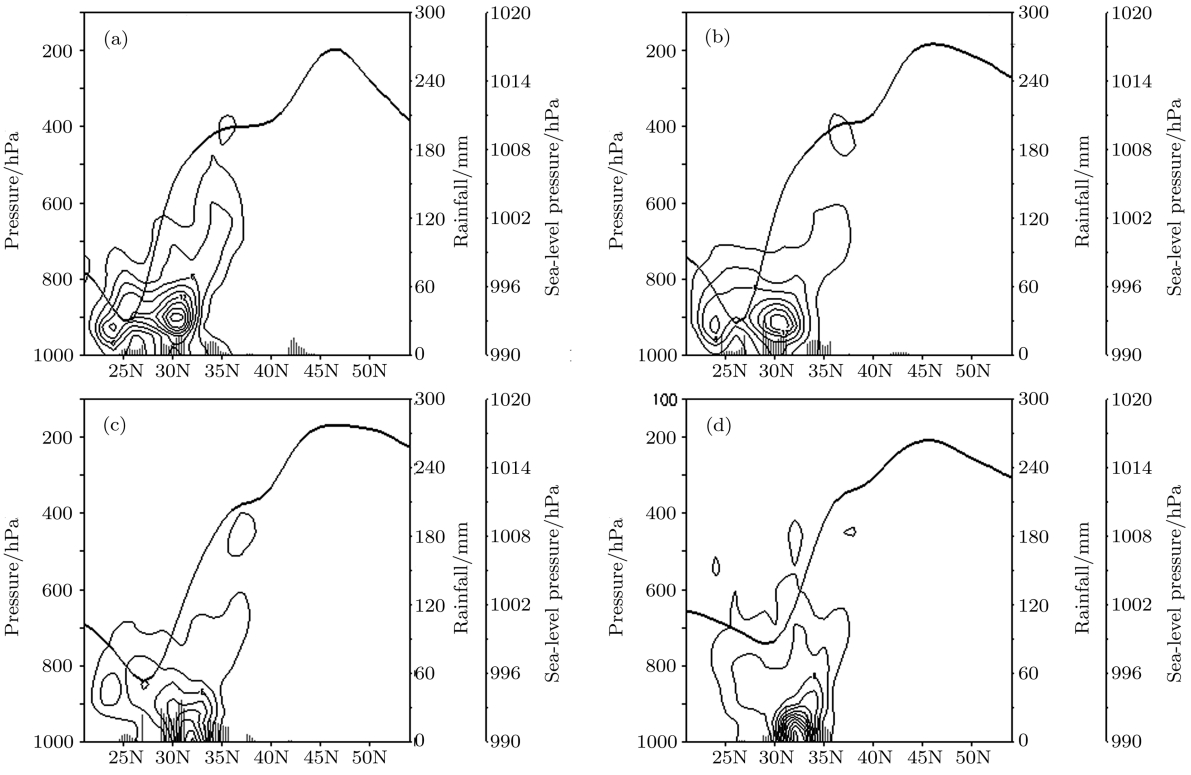


Fig. 2. The horizontal distributions of $\langle |M| \rangle$ (solid contour, unit: 10^{-3} K$\cdot$s^{-1}, observed 6 h accumulative rainfall (grey shade, unit: mm) and horizontal velocity vector perturbation on 850 hPa level (unit: m$\cdot$s^{-1}) at 12 UTC (a), 18 UTC 18 (b), 00 UTC (c), 06 UTC (d), 12 UTC (e), 18 UTC 19 (f), 00 UTC (g) and 06 UTC 20 (h) Sep. 2007. The ordinate is the latitude and the abscissa is the longitude.

The above analysis of $\langle|M|\rangle$, sea-level pressure and observed rainfall revealed that the TSAP ($\langle|M|\rangle$), presenting a spiral-band pattern in horizontal distribution, cooperated well with the observed 6 h accumulative rainband that originated in the northern edge of 'Wipha' and stretched northeastwards. This indicated that the rainband was closely related to $\langle|M|\rangle$ and they corresponded with each other. The reasonable explanation to this may be that the active wave represented by $\langle|M|\rangle$ over the observed rianband was the chief weather system resulting in heavy rainfall. In addition, the low-pressure centre shifted along the spiral-band channel of $\langle|M|\rangle$.

The meridional-vertical cross sections of TSAP, sea-level pressure and observed 6 h accumulative rainfall were presented in Fig. 3. As it was shown, the rainband over the latitudes of 24°N–36°N lays in the north of low-pressure centre at 12 UTC 18. The anomaly of $|M|$ chiefly appeared in the middle-lower troposphere below 700 hPa and laid over the rainband. The $|M|$ reached its maximum near (30°N, 900 hPa). After that, the low-pressure centre moved northwards and gradually became shallow. Keeping the same phase with the low-pressure centre, the high value of $|M|$ was located in the boundary layer below 850 hPa. The rainband was perched under the centre of $|M|$. The fact that the $|M|$ over the observed rainband was anomalous in the lower troposphere suggested that the wave or disturbance over the observed rainband, being closely related to the precipitable system, was very active in the boundary layer during the landfall-typhoon heavy-rainfall event.

To inspect the composition structure of $|M|$, we analyse the two composed portions of the perturbation scalar M, PVC and CHV, and shown them in Figs. 4 and 5. As it was shown in Fig. 4, at 12 UTC 18 before 'Wipha' landed, the anomalous-value areas of M, PVC and CHV mainly appeared over the observed rainband in the lower-level troposphere. The PVC was negative above 950 hPa level and positive below 950 hPa level. Its negative value was much larger than its positive value in magnitude. The CHV mainly appeared positive above 950 hPa level. Opposite to PVC in sign above 950 hPa level, CHV was smaller than PVC in magnitude. Thus, the sum of the two portions was still negative above 950 hPa level over the observed rainband, which indicated that PVC was the primary composed portion of M. It can be inferred that M represented the property of PVC. At 12 UTC 19 after 'Wipha' landed (Fig. 5), M, PVC and CHV were anomalous in the lower-level troposphere over the observed rainband. The centre of M was positive below 900 hPa level and its central pressure



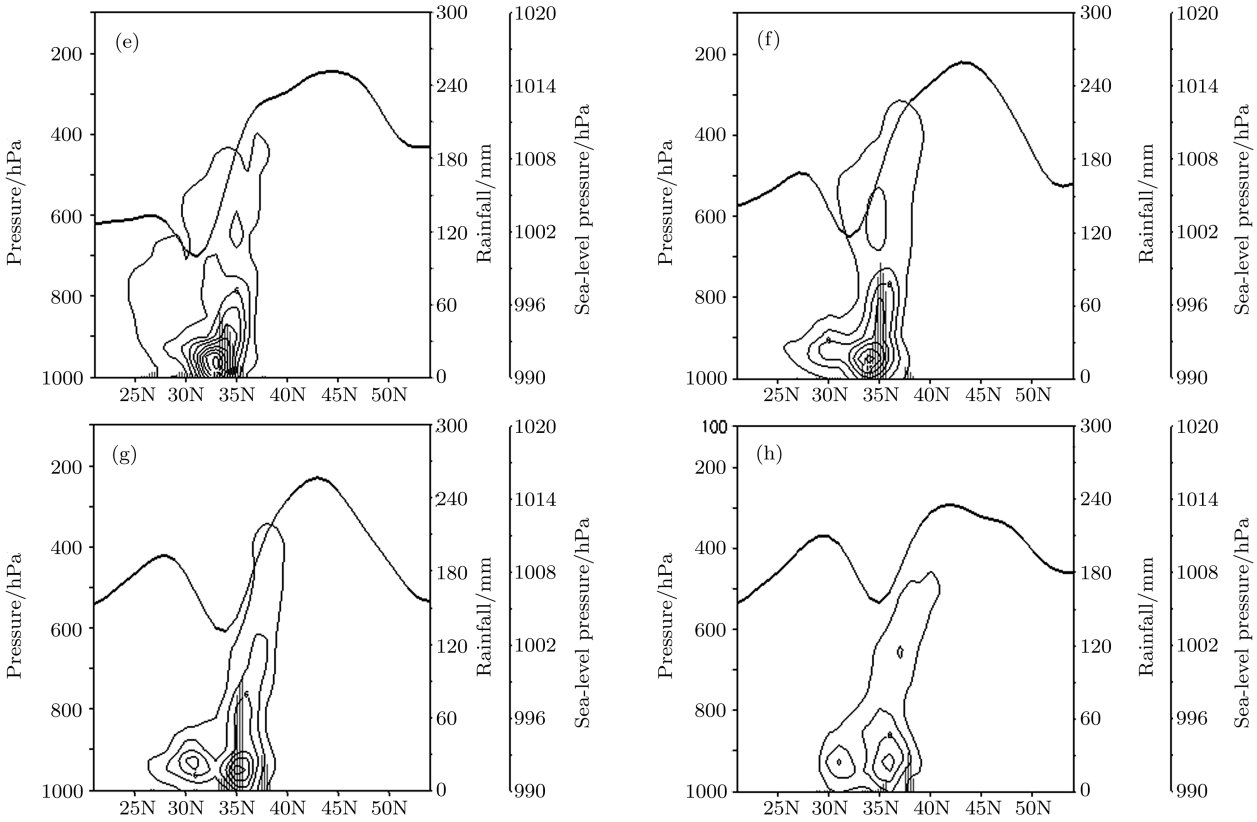


Fig. 3. The meridional-vertical cross sections along 120°E of $|M|$(the solid contour, unit: 10^{-8} K·s^{-1}Pa^{-1}) at 12 UTC (a), 18 UTC 18 (b), 00 UTC (c), 06 UTC (d), 12 UTC (e), 18 UTC 19 (f), 00 UTC (g) and 06 UTC 20 (h) Sep. 2007. The thick solid line denotes the sea-level pressure (unit: hPa) and the bar denotes the observed 6 h accumulative rainfall (unit: mm). The ordinate is the pressure and the abscissa is the latitude.

descended to 975 hPa. The positive value of PVC below 900 hPa level was larger than its negative value above 900 hPa level in magnitude. The CHV was positive below 900 hPa level and was comparative to the positive-value PVC. Thus, the sum of the two portions below 900 hPa level represented the cooperation of PVC and CHV, while the negative value of M above 900 hPa level embodied the negative-value PVC.

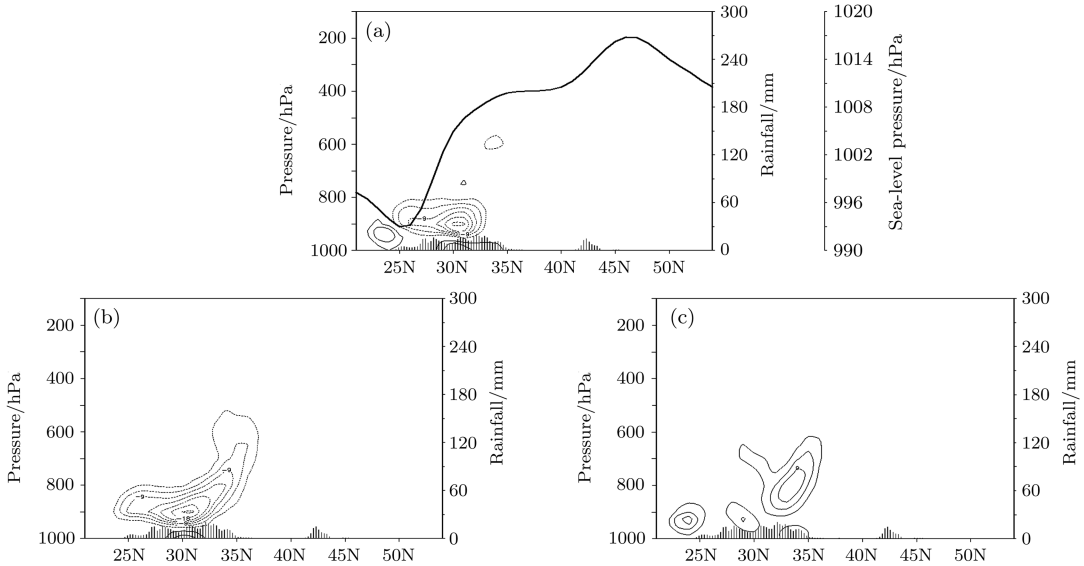


Fig. 4. The meridional-vertical cross sections along 120E of M (a), the solid contour, unit 10^{-8} K·s^{-1}Pa^{-1}; PVC (b), the solid contour, unit 10^{-8} K·s^{-1}Pa^{-1} and CHV (c), the solid contour, unit 10^{-8} K·s^{-1}Pa^{-1} at 12 UTC 18 Sep. 2007. The thick solid line denotes the sea-level pressure (unit: hPa) in (a) and the bar denotes the observed 6 h accumulative rainfall (unit: mm). The ordinate is the pressure and the abscissa is the latitude.

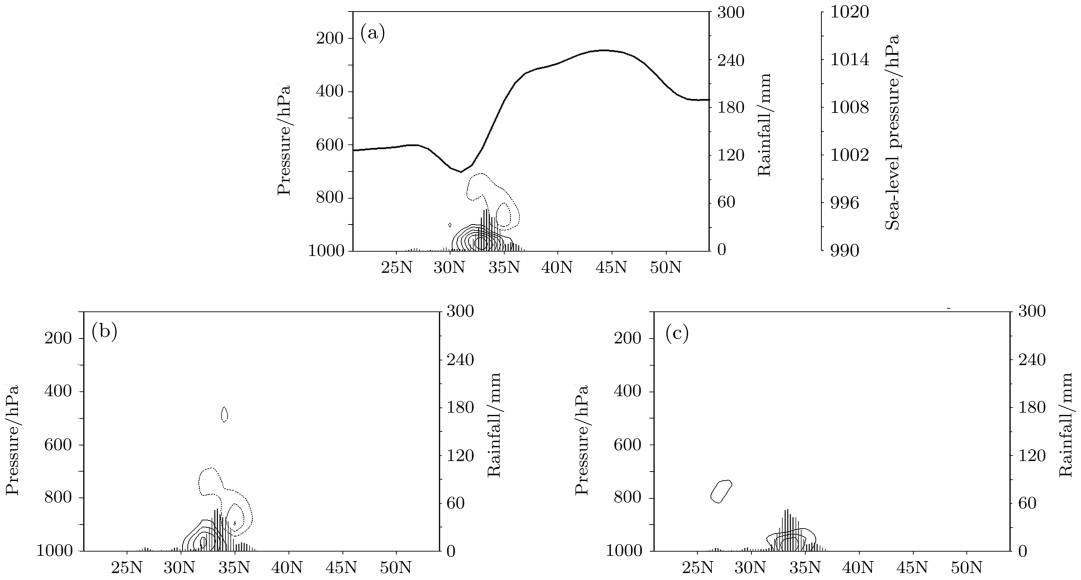


Fig. 5. The same as Fig. 4 except at 12 UTC 19 Sep. 2007.

To examine the important dynamic factors responsible for the variation of $\langle|M|\rangle$, the wave-activity flux divergence ($\nabla\cdot\boldsymbol{F}$) in Eq. (31) vertically integrated was calculated with the NCEP/NCAR global final analysis data. Since the data was coarse in temporal resolution and did not include enough information of diabatic heating, the local change of $\langle|M|\rangle$ and source or sink for $|M|$ were excluded from evaluation. The horizontal distributions of $\langle\nabla\cdot\boldsymbol{F}\rangle$ and its five composed portions were presented in Figs. 6 and 7. As it was shown, $\langle\nabla\cdot\boldsymbol{F}\rangle$ and its five composed portions appeared anomalous over the observed rainband at 12 UTC 18 (Fig. 6). At 12 UTC 18 before 'Wipha' made landfall, $\langle\nabla\cdot\boldsymbol{F}_1\rangle$ was larger than the other four portions in magnitude, indicating that the advection of $|M|$ by basic-state flow made primary contribution to the tendency of $\langle|M|\rangle$. The $\langle\nabla\cdot\boldsymbol{F}_4\rangle$ exerted stronger influence than $\langle\nabla\cdot\boldsymbol{F}_2\rangle$, $\langle\nabla\cdot\boldsymbol{F}_3\rangle$ and $\langle\nabla\cdot\boldsymbol{F}_5\rangle$ on the local change of $\langle|M|\rangle$ over the rainband. This meant that the coupling of general potential temperature perturbation with curl of Coriolis force perturbation was another important dynamic factor answering for the evolution of $\langle|M|\rangle$. Although the magnitudes of $\langle\nabla\cdot\boldsymbol{F}_2\rangle$, $\langle\nabla\cdot\boldsymbol{F}_3\rangle$ and $\langle\nabla\cdot\boldsymbol{F}_5\rangle$ were smaller than those of $\langle\nabla\cdot\boldsymbol{F}_1\rangle$ and $\langle\nabla\cdot\boldsymbol{F}_4\rangle$, the three terms were not negligible in some local rainfall regions.

At 12 UTC 19 after the typhoon made landfall, the observed rainband still lays in the anomalous regions of $\langle\nabla\cdot\boldsymbol{F}\rangle$ and its five composed portions (Fig. 7). It could be seen that all of the five composed portions contributed to the local change of $\langle|M|\rangle$. This implied that after the typhoon landed, besides the above mentioned two dynamic factors, there were another three primary dynamic factors responsible for the tendency of $\langle|M|\rangle$, namely, the coupling of general potential temperature perturbation with covariance between basic-state flow and velocity perturbation, the interaction between the basic-state general potential temperature advection by velocity vector perturbation and vertical shear of velocity perturbation, and the interaction between general potential temperature perturbation and horizontal gradients of geopotential height perturbation. Different from the situation at 12 UTC 18, $\langle\nabla\cdot\boldsymbol{F}_1\rangle$ was weakened and the other four portions $\langle\nabla\cdot\boldsymbol{F}_2\rangle$, $\langle\nabla\cdot\boldsymbol{F}_3\rangle$, $\langle\nabla\cdot\boldsymbol{F}_4\rangle$ and $\langle\nabla\cdot\boldsymbol{F}_5\rangle$ to a degree were enhanced over the rainfall regions. Especially, the increases of $\langle\nabla\cdot F_2\rangle$, $\langle\nabla\cdot\boldsymbol{F}_3\rangle$ and $\langle\nabla\cdot\boldsymbol{F}_5\rangle$ near the rainfall centre (33°N, 119°E) were remarkable. The phase of $\langle\nabla\cdot\boldsymbol{F}_5\rangle$ was opposite to that of $\langle\nabla\cdot\boldsymbol{F}_2\rangle$, $\langle\nabla\cdot\boldsymbol{F}_3\rangle$ and $\langle\nabla\cdot\boldsymbol{F}_4\rangle$, indicating that the forcing term associated with horizontal gradients of geopotential height perturbation made a contribution which was opposite to that of the other three primary dynamic factors near the rainfall centre. Furthermore, $\langle\nabla\cdot\boldsymbol{F}\rangle$ near the rainfall centre mainly reflected the integrative character of $(\langle\nabla\cdot\boldsymbol{F}_2\rangle+\langle\nabla\cdot\boldsymbol{F}_3\rangle+\langle\nabla\cdot\boldsymbol{F}_4\rangle+\langle\nabla\cdot\boldsymbol{F}_5\rangle)$, and the influence from the advection of $|M|$ by basic-state flow was weakened over the rainband.

It can be seen from the above analysis that $|M|$ was capable of indicating the vertical dynamic and thermodynamic structure of disturbance in lower-level

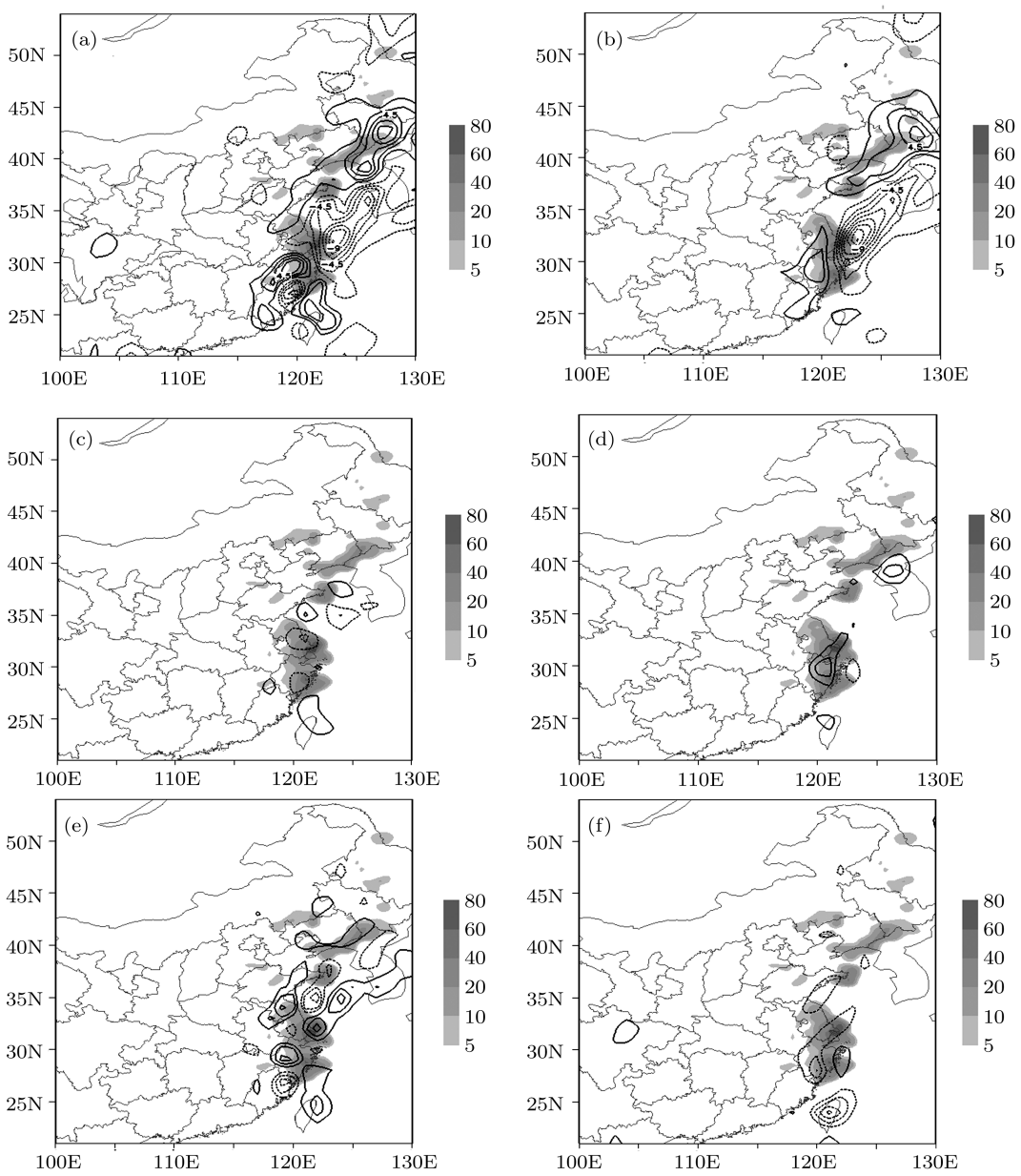


Fig. 6. The horizontal distributions of $\langle \nabla \cdot \boldsymbol{F} \rangle$ (a), $\langle \nabla \cdot \boldsymbol{F}_1 \rangle$ (b), $\langle \nabla \cdot \boldsymbol{F}_2 \rangle$ (c), $\langle \nabla \cdot \boldsymbol{F}_3 \rangle$ (d), $\langle \nabla \cdot \boldsymbol{F}_4 \rangle$ (e) and $\langle \nabla \cdot \boldsymbol{F}_5 \rangle$ (f) at 12 UTC 18 Sep. 2007 (contour, unit: 10^{-8} K$\cdot$s^{-2}). The grey shade denotes the observed 6 h accumulative rainfall/mm. The ordinate is the latitude and the abscissa is the longitude.

troposphere over the observed rainband so that $|M|$ corresponded well with the observed 6 h accumulative rainfall. Therefore, $|M|$ might be regarded as a good tracer detecting the precipitable weather system. Before the typhoon landed, the dynamic processes associated with the advection of $|M|$ by basic-state flow and Coriolis force perturbation over the observed rainband were primarily responsible for the evolution of $|M|$. After the typhoon landed, the contribution from the advection of $|M|$ by basic-state flow was weakened, but the other four forcing terms were enhanced.

4. Discussion

On the basis of previous studies, a perturbation scalar combining the PVC with the CHV is introduced. The absolute value of the perturbation scalar quadric in disturbance fields is referred to as the TSAP. Because the new parameter is always definitely positive in sign, it is capable of describing a kind of perturbation energy and represents disturbance strength. The tendency equation of the parameter is also derived from the primitive

equations in pressure coordinates. Since the tendency equation takes on a local flux form and its all terms are quadric in disturbance fields except the source or sink, the equation in nature is a wave-activity law.

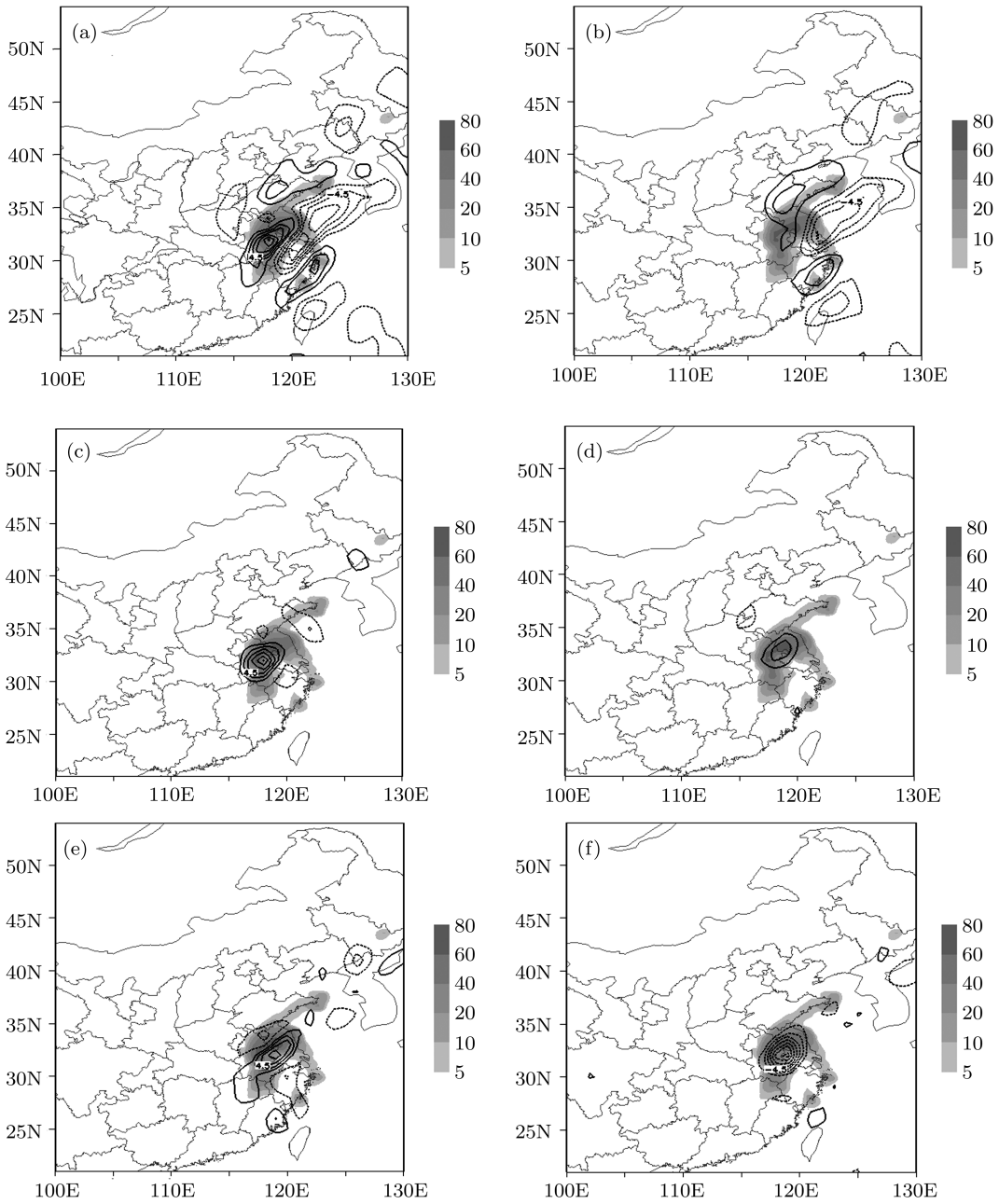


Fig. 7. The same as Fig. 6 except at 12 UTC 19 Sep. 2007.

The parameter was employed to diagnose dynamic process over the observed rainband of landfall typhoon 'Wipha' with the NCEP/NCAR global final analysis data. The analysis showed that the parameter was able to describe the typical vertical dynamic and thermodynamic structure characters over the observed 6 h accumulative rainband so that it coincided with the observed rainband in spatial distribution pattern and temporal evolution trend. This suggested that there existed a band of disturbance in lower troposphere over the observed rainband which is primary precipitable weather system. Before the typhoon landed, the disturbance primarily came from the perturbation vertical component of convection vorticity vector and was driven by the two primary dynamic processes, namely, the advection of TSAP by

basic-state flow and the coupling of general potential temperature perturbation with curl of Coriolis force perturbation. After the typhoon landed, besides PVC, CHV also made partial contribution to the disturbance. The five primary dynamic processes presented by the five component portions of $\nabla \cdot \boldsymbol{F}$ were responsible for the evolution of TSAP after the landfall of 'Wipha'. The four terms, which were associated with the coupling of general potential temperature perturbation with covariance between basic-state flow and velocity perturbation, the basic-state general potential temperature advection by velocity vector perturbation, the curl of Coriolis force perturbation and the horizontal gradients of geopotential height perturbation, were enhanced while the advection of TSAP by basic-state flow was weakened.

Since TSAP is closely related to the observed surface rainfall, the parameter may be used as a dynamic factor to predict the location of heavy rainfall. For example, we may use the forecasting fields of the global forecast system (GFS) in NCEP to calculate TSAP. Following the above obtained relation between TSAP and observed surface rainfall, it can be judged that the location where TSAP has high-value is the strong precipitation region. Since the GFS provides the 0–180 hour forecast fields, TSAP may predict the precipitation before 0–180 hours.

References

[1] Zhou Y S, Cao J and Gao S T 2008 *Acta Phys. Sin.* **57** 6654 (in Chinese)

[2] Huang S X, Cai Q F, Xiang J and Zhang M 2007 *Acta Phys. Sin.* **56** 3022 (in Chinese)

[3] Cao J, Gao S T and Zhou Y S 2008 *Acta Phys. Sin.* **57** 2600 (in Chinese)

[4] Chen Z, Yang K and Wu H 2009 *Acta Phys. Sin.* **58** 4362 (in Chinese)

[5] Wu R S and Tan Z M 1989 *Acta Meteorol. Sin.* **47** 436 (in Chinese)

[6] Li Y D, Liu J and Gao S 2005 *Meteorol. Sci. Tech.* **33** 7 (in Chinese)

[7] Yang Y, Liu Y, Wan Z, Wu B and Shen W 1994 *Acta Meteorol. Sin.* **52** 379 (in Chinese)

[8] Wu B, Xu C, Liu Y, Zhou L, Yu Y, Wei D and Chen L 1996 *Quart. J. Appl. Meteorol.* **7** 108 (in Chinese)

[9] Li Y and Shou S 1999 *J. Nanjing Institute of Meteorol.* **22** 95 (in Chinese)

[10] Ertel H 1942 *Meteorol. Zeitschr Braunschweigs* **6** 277

[11] Wu G, Cai Y and Tang X 1995 *Acta Meteorol. Sin.* **53** 387 (in Chinese)

[12] Gao S, Lei T, Zhou Y and Dong M 2002 *Quart. J. Appl. Meteorol.* **13** 662 (in Chinese)

[13] Bi B, Liu Y and Li Z 2005 *Chin. J. Atmosph. Sci.* **29** 814 (in Chinese)

[14] Chen Z, Gao W, Min W and He G 2006 *Plateau Meteorol.* **25** 983 (in Chinese)

[15] Gao S, Ping F, Li X and Tao W K 2004 *J. Geophys. Res.* **109** D14106 doi:10.1029/2004JD004807

[16] Gao S, Cui X, Zhou Y, Li X and Tao W K 2005 *J. Geophys. Res.* **110** D17104 doi:10.1029/2004JD005675

[17] Gao S, Li X, Tao W K, Shie C L and Lang S 2007 *J. Geophys. Res.* **112** D01105 doi:10.1029/2006JD007179

[18] Cui X P 2008 *Chin. Phys.* B **17** 2304

[19] Gao S, Wang X and Zhou Y 2004 *Geophys. Res. Lett.* **31** L12113 doi:10.1029/2003GL019152

[20] Wang P and Dai X G 2005 *Acta. Phys. Sin.* **54** 4961 (in Chinese)

[21] Dai X G, Fu C B and Wang P 2005 *Chin. Phys.* **14** 850

[22] Wang P and Dai X G 2004 *Chin. Phys.* **13** 1770

[23] Ran L and Boyd J P 2008 *Chin. Phys.* B **17** 1138